University of Groningen

Transcutaneous immunization via dissolving microneedles protects mice from lethal influenza H7N9 virus challenge

Liu, Siqi; Yang, Guozhong; Li, Minghui; Sun, Fang; Li, Yufeng; Wang, Xiliang; Gao, Yunhua; Yang, Penghui

Link to publication in University of Groningen/UMCG research database
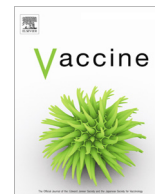
Transcutaneous immunization via dissolving microneedles protects mice from lethal influenza H7N9 virus challenge

Siqi Liu [a,b], Guozhong Yang [c], Minghui Li [d], Fang Sun [a], Yufeng Li [a], Xiliang Wang [d], Yunhua Gao [c,*], Penghui Yang [a,*]

[a] *The First Medical Center of Chinese PLA General Hospital, Beijing 100835, China*
[b] *Department of Rheumatology and Clinical Immunology, University Medical Center Groningen and University of Groningen, Hanzeplein 1, P.O. Box 30.001, 9700 RB Groningen, NL, the Netherlands*
[c] *Key Laboratory of Photo Chemical Conversion and Optoelectronic Materials, Technical Institute of Physics and Chemistry, Chinese Academy of Sciences, Beijing, China*
[d] *State Key Laboratory of Pathogens and Biosecurity, Beijing Institute of Microbiology and Epidemiology, Beijing 100071, China*

ARTICLE INFO

ABSTRACT

Avian influenza H7N9 virus has first emerged in 2013 and since then has spread in China in five seasonal waves. In humans, influenza H7N9 virus infection is associated with a high fatality rate; thus, an effective vaccine for this virus is needed. In the present study, we evaluated the usefulness of dissolving microneedles (MNs) loaded with influenza H7N9 vaccine in terms of the dissolution time, insertion capacity, insertion depth, and structural integrity of H7N9 virus *in vitro*. Our *in vitro* results showed MNs dissolved within 6 mins. The depth of skin penetration was 270 μm. After coating with a matrix material solution, the H7N9 proteins were agglomerated. We detected the H7N9 delivery time and humoral immune response in vivo. In a mouse model, the antigen retention time was longer for MNs than for intramuscular (IM) injection. The humoral response showed that similar to IM administration, MN administration increased the levels of functional and systematic antibodies and protection against the live influenza A/Anhui/01/2013 virus (Ah01/H7N9). The protection level was determined by the analysis of pathological sections of infected lungs. MN and IM administration yielded results superior to those in the control group. Taken together, these findings demonstrate that the use of dissolving MNs to deliver influenza H7N9 vaccines is a promising immunization approach.

© 2022 Published by Elsevier Ltd.

1. Introduction

A new virus named avian influenza A (H7N9) was detected in humans in China at the end of March 2013 [1]. In total, 436 confirmed H7N9 infections, resulting in 167 deaths, were documented between March 2013 and July 2014 [2]. Between 2013 and 2017, five epidemic waves of H7N9 infection occurred in China, with an approximate fatality rate of 40% [3]; the virus also spread to other countries [4]. Most cases of H7N9 infection are acquired due to exposure to poultry; direct human to human transmission occurs less commonly. As H7N9 accumulates mutations during its spread, its genetic diversity and population size increased after the five epidemic waves [5]. The clinical manifestations of H7N9 infection include rapidly developing pneumonia, leukopenia, lymphopenia, increased cytokine and chemokine levels. High cytokine and chemokine levels were particularly prominent in fatal cases [6]. H7N9 infection has a mortality rate of up to 38% [7] and has the potential to cause a pandemic. Thus, the development of prevention and control measures for H7N9 infection is essential.

Vaccination is the most effective means of preventing influenza infection. Three candidate vaccines were identified in 2017 [8]: a reverse genetics-based H5/H7 bivalent inactivated vaccine, a Newcastle disease virus vectored HA vaccine, and a duck enteritis virus vectored HA vaccine. A DNA-based vaccine has also been developed [9]. In addition, a virus-like particle (VLP) vaccine has demonstrated safety and immunogenicity against H7N9 influenza [10], but its manufacturing process needs to be improved to achieve efficacy against multiple variants and subtypes of the virus. Intramuscular (IM) injection has several disadvantages, including low

---

vaccination coverage, high immunization cost, and the wasting of medical resources. Microneedles (MNs) have recently been used for transcutaneous immunization, and this approach has several advantages, such as the avoidance of needle phobia and harmful material deposition [11]. The abundance of dermal Langerhans dendritic cells enables vaccine delivery through the skin [12]. Dissolving MNs have been used in cosmetic products and human trials [13,14]. Our previous study showed that transcutaneous immunization with recombinant Staphylococcal enterotoxin B protein using MNs protects against lethal enterotoxin challenge [15]. Other studies have shown that MNs are useful for the delivery of a VLP-based EV71 vaccine [16], a polio vaccine [17], and cancer immunotherapy [18].

In the present study, we used influenza virus H7N9 as a model antigen applied on MNs to investigate whether MNs could induce an effective immune response and protection. Then, we compared the immune effects of vaccination using MNs and IM administration in a mouse model. Finally, we evaluated the protective efficacy of these vaccines using a wild type influenza A/Anhui/01/2013 virus (Ah01/H7N9) challenge.

2. Materials and methods

2.1. Fabrication of H7N9 loaded dissolving MN

The influenza virus A/Anhui/1/2013 (H7N9) was incubated in chicken eggs, purified using sucrose density gradient centrifugation, and inactivated with 0.04% formalin. Then, dialysis was performed to remove the excess formalin. The inactivated H7N9 virus was used as the vaccine antigen. The experiments involving viruses were conducted in biosafety level III laboratories.

H7N9-loaded dissolving MNs were fabricated using micromolding, as reported previously [15]. In total, 7 μg influenza H7N9 vaccine protein was loaded onto each MN patch (measured by BCA protein assay kit; $R^2 = 0.998$). The matrix solution contained chondroitin sulfate, hydroxypropyl methylcellulose and trehalose. Rhodamine B labeled dissolving MNs loaded with Cy-7-labeled H7N9 were processed using a similar procedure.

2.2. In vitro evaluation of H7N9-loaded MN dissolution ability

H7N9 loaded MNs were inserted into porcine skin and removed after 0, 1, 3, or 6 min. Then, the ability of the MNs to dissolve was evaluated under optical microscope (Olympus, Tokyo, Japan).

2.3. Evaluation of H7N9-loaded dissolving MN insertion under frozen section

Rhodamine B labeled dissolving MNs were applied to ex vivo porcine ear skin (Linxi Jingde Agricultural Products Sales Co., Ltd., Hebei, China) for 3 min and then removed. The removed tissue was placed in a microtome, infiltrated into an optimal cutting temperature compound (Tissue-Tek; Sakura, Torrance, CA, USA), and frozen in liquid nitrogen. Subsequently, the microtome part of a cryostat (Leica, Bensheim, Germany) was used to cut 9-μm-thick frozen sections, which were placed on a glass slide, stained, and observed under a microscope and fluorescence microscope (Olympus, Tokyo, Japan).

2.4. Confocal laser scanning microscopic evaluation of H7N9-loaded dissolving MN insertion depth

Cy-7 labeled H7N9 loaded dissolving MNs were applied to porcine ear skin for 3 mins and then removed. The skin was placed on a glass slide and photographed under a confocal laser scanning microscope (CLSM; Nikon, Tokyo, Japan). The specimens were scanned from the surface layer to the deep layer at 20 mm intervals to determine the MN insertion depth. Confocal images were presented in an xyz plane for three dimensional (3D) visualization.

2.5. Assessment of the structural integrity of H7N9 vaccine coated with MN matrix solution

H7N9 protein and MN coating matrix solution were mixed overnight. Native H7N9 (as a control) and the H7N9 mixture were fixed on the next day and observed under an electron microscope (EM).

2.6. Assessment of H7N9-loaded MN particle size distribution

Influenza virus H7N9 antigen (as a control) and H7N9-loaded MNs were dissolved in 0.5 mL phosphate buffered saline (PBS) and evaluated using dynamic light scattering (DLS). A Zetasizer NanoZS particle analyzer (Malvern Instruments Ltd., Malvern, UK) was used to analyze the particle size distribution. The concentration of the H7N9 control solution was maintained similar to the H7N9 loaded MN solution.

2.7. Assessment of H7N9 distribution in vivo

The abdomens of 8-week-old female BALB/c mice (18–20 g; n = 3) were shaved using depilatory cream. Cy-7 labeled MNs were inserted into the mice's skin for 5 min and then removed. An equal dose of H7N9 vaccine was injected into the hind leg muscle of each mouse (i.e., IM administration). The mice were anesthetized with 1% pentobarbital sodium and observed using an in vivo imaging system (IVIS; PerkinElmer, USA) at 6 h, 3, 5, and 8 days to collect fluorescence data. Fluorescence signals in regions of interest (ROIs) were quantified using Living Image 3.0.

2.8. In vitro immunization of mice

2.8.1. Immunization schedule

All procedures involving animals were approved by the Institute of Animal Care and Use Committee of the Chinese PLA General Hospital (Beijing, China). The animal study was performed in accordance with the recommendations of the Guide for the Care and Use of Laboratory Animals of the Chinese PLA General Hospital.

The immunization schedule was shown in Supplementary Fig. 1. Female BALB/c mice (6–8 weeks old) were purchased from the Laboratory Animal Center and divided into three groups: MN, IM, and Control (PBS; n = 6 each). The mice were immunized using two doses of vaccine administered at a 21 day interval. Mice in the MN and IM groups received the same dose of inactivated H7N9 virus vaccine with a protein content of 7 μg (BCA protein assay kit; $R^2 = 0.998$). Mice in the control group received 100 μL PBS. Mice in the IM group received the H7N9 vaccine solution (7 μg/100 μL/dose) injection into the hind leg muscle of each mouse. For MN injection, the hair on the abdomen was removed 1 day before vaccination. The mice were anesthetized using isoflurane inhalation; then, the abdominal skin was stretched, the MNs were applied, and the skin was held for 10 mins. On day 14 after booster immunization, blood samples were collected by retroorbital bleeding, then serum samples were stored at −20 °C until use.

2.8.2. Hemagglutination inhibition test

A hemagglutination inhibition (HI) assay to detect antibody against H7N9 was performed following the standard procedure. Briefly, mouse serum was mixed with receptor-destroying enzyme (Denka-Seiken, Tokyo, Japan) at a 1:3 ratio at 37 °C for 19 h, and then at 56 °C for 1 h. Samples were serially diluted in 25 μL PBS

in wells. Then, 25 µL H7N9 antigen (4 HA units) was added to the wells and incubated for 30 min at room temperature. Subsequently, 1% chicken erythrocyte suspension was added to the wells, and the plates were incubated for 30 min at room temperature. The HI titer was expressed as the reciprocal value of the highest serum dilution that completely inhibited hemagglutination.

2.8.3. Detection of serum antibody responses

Influenza specific immunoglobulin G (IgG) antibody levels were measured by enzyme-linked immunosorbent assay (ELISA). Briefly, 96-well plates (Thermo Fisher, USA) were coated with influenza H7N9 antigen solution overnight at 4 °C. The plates were blocked with 2% bovine serum albumin (BSA; Sigma-Aldrich, St. Louis, MO, USA) in PBS with 0.1% Tween™ 20 for 2 h at 37 °C. Then, the plates were incubated with 50 µL serially diluted serum samples for 2 h. After washing three times, the plates were incubated with 50 µL of a 1:20,000 dilution of horseradish peroxidase conjugated goat anti-mouse IgG, IgG1, and IgG2a antibodies (Sigma-Aldrich) for 1 h. Goat anti rat IgG (Sigma-Aldrich) was used as the secondary antibody. The plates were washed four times, and the antibody level was quantified by adding 50 µL TMB substrate. After 15 min, the reaction was terminated by adding 50 µL 2 mol/L H_2SO_4, and the optical density was measured at 450 nm.

2.8.4. Enzyme-linked immunosorbent spot assay

Interleukin-4 (IL-4) and interferon-gamma (IFN-γ) enzyme-linked immunosorbent spot (ELISPOT) kits (BD Biosciences, San Diego, CA, USA) for mice were used for the ELISpot assays. Mouse spleens were harvested aseptically 2 weeks after booster immunization. The peripheral blood mononuclear cells (PBMCs) were collected from splenocytes using lymphocyte separation medium (Dakewei, Beijing, China) at a density of 2×10^6/mL. The influenza H7N9 vaccine (5 µg/mL) was added to each well and incubated for 24 h in a humidified incubator at 37 °C and 5% CO_2. The plates were washed and processed according to the manufacturer's protocol. Spots were scanned using an ELISpot plate reader system (Cellular Technology Ltd., Cleveland, OH, USA). The results were expressed as the number of spot forming cells per 10^5 PBMCs.

2.9. Virus challenge

Another group set of female BALB/c mice (6–8 weeks old) (n = 9) were immunized in the same schedule for the virus challenge study (see Supplementary Fig. 1). At 2 weeks after boost, mice in each group (n = 9) were inoculated intranasally with a median tissue culture infectious dose (0.7 × 10⁶ PFU (plaque forming unit)/ml measured by TCID50) of the live influenza A/Anhui/01/2013 virus (Ah01/H7N9) (0.7 × 10⁶ PFU/ml in 50 µL volume diluted in PBS). The mice (n = 6) were observed for illness, weight loss, and death after the challenge. On day 4 after inoculation, lavage fluid was harvested from the rest mice's lungs (n = 3) and used to detect virus titers by TCID50 assay, performed as described previously [19], virus titers were estimated based on the method proposed by Reed and Muench. Their lungs were separated and fixed in 4% formalin, dehydrated in increasing ethanol concentrations, embedded in paraffin, sectioned, and stained with hematoxylin and eosin. Histopathological photographs were obtained using an optical microscope (10 × magnification, Leica, Germany).

2.10. Statistical analysis

Analysis of variance and unpaired Welch's correction were used to analyze the HI, IgG, and virus titer data with SPSS software (version 19.0; IBM Corp, Armonk, NY, USA). Results are presented as means ± standard deviations. $p < 0.05$ was considered to indicate significance.

3. Results

3.1. Fabrication, characteristics, and insertion parameters of dissolving MNs for the influenza H7N9 vaccine

The MNs were fabricated using chondroitin sulfate, hydroxypropyl methylcellulose, and trehalose. Rhodamine B is a fluorescent compound with an excitation peak at 546 nm and an emission peak at 568 nm, and it can be used to track the needle penetration depth under digital microscope and CLSM. The rhodamine B loaded dissolving MNs were pink. (Fig. 1A and B; an MN with 196 needles per array is about the size of a 1 yuan coin). Fig. 1C shows the MN arrays under a stereomicroscope (Nikon, Japan). Fig. 1D shows the needle length before and 1, 3, and 6 mins after MN application to mouse skin under optical microscope (Olympus, Japan); the needles were inserted into the skin and dissolved after 6 mins.

A recent study showed that the insertion of dissolving MNs could be influenced by several factors, such as their geometry and physical characteristics, and the temperature used during fab-
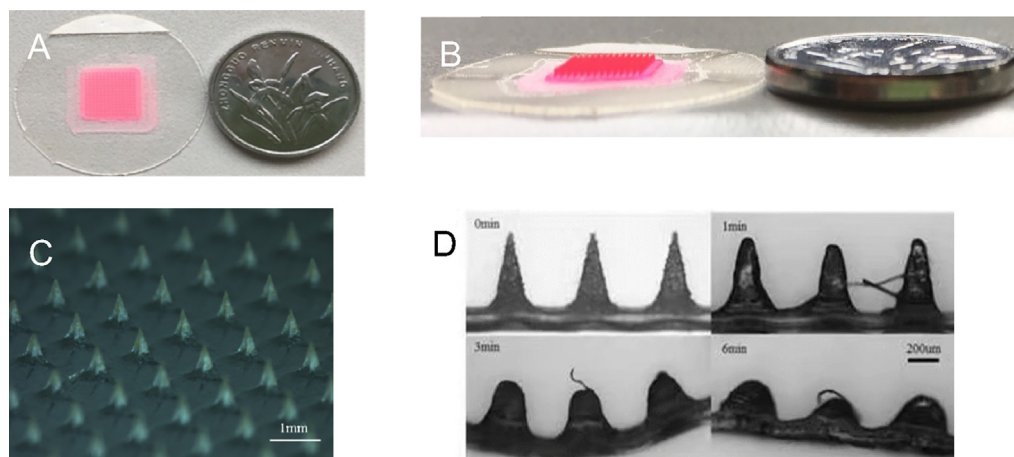
**Fig. 1. Dissolving microneedles (MNs) loaded with inactivated H7N9 vaccine.** (A, B) Top and side views of the dissolving MNs, with a 1 yuan coin provided for scale. (C) Digital image of an MN array patch under a stereomicroscope (5 × magnification, Nikon, Japan). (D) Depth of H7N9 vaccine loaded MNs in the skin before and 1, 3, and 6 min after administration (10 × magnification under optical microscope (Olympus, Japan)).
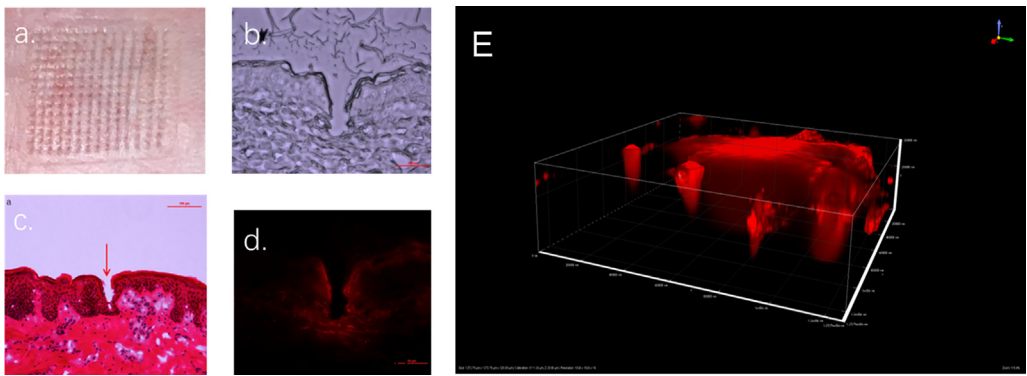
Fig. 2. Insertion capacity of dissolving microneedles (MNs). (A) Site of skin penetration by the MNs. (B) Microscopic image of the porcine skin surface after application of the MN patch. (C) Optical microscopic image of the hematoxylin and eosin stained porcine skin surface after application of the MN patch. (D) Fluorescence micrograph of the porcine skin after the application of dissolving MNs loaded with rhodamine. (E) Confocal image and three dimensional graph of the H7N9 loaded MNs.
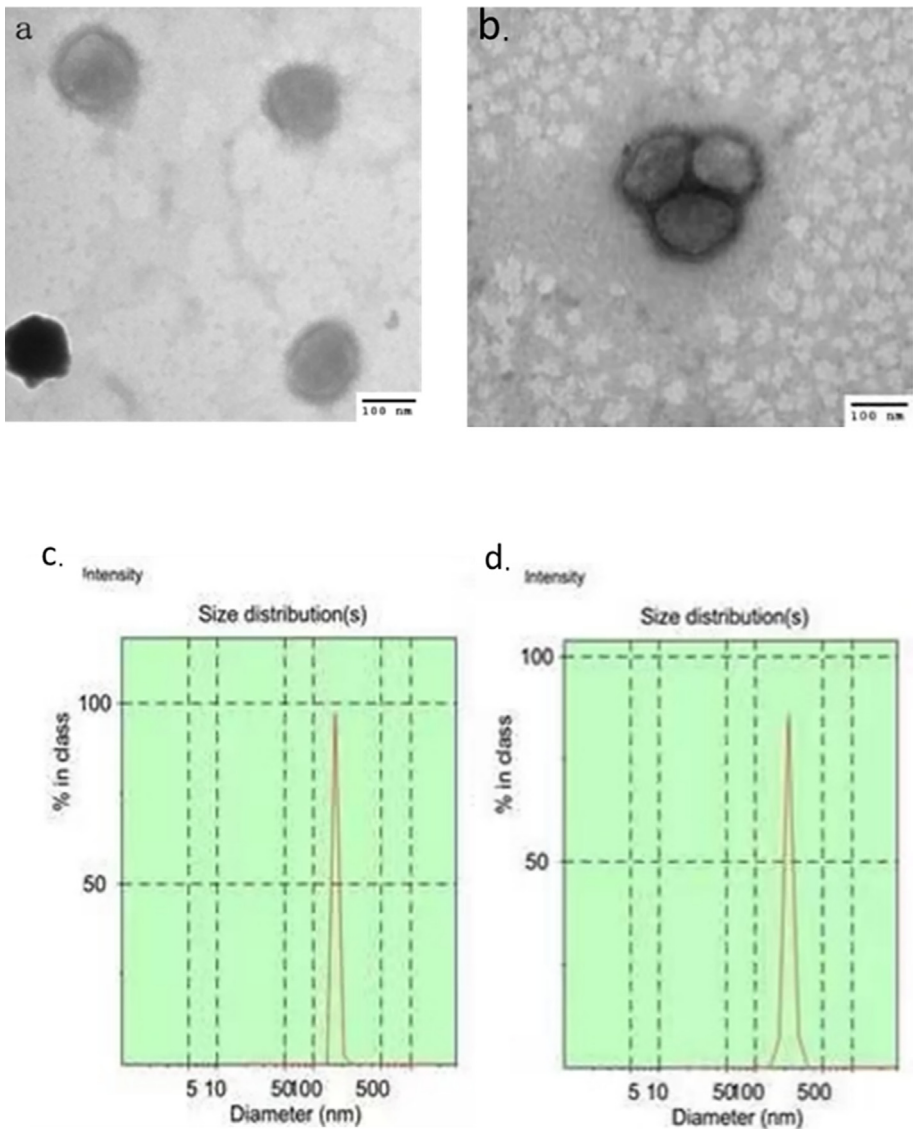
Fig. 3. Particle size distribution. Particle size distribution was assessed using electron microscopy for (A) native influenza H7N9 antigen protein solution and (B) microneedle (MN) material solution. Dynamic light scattering analyses of (C) the native influenza H7N9 antigen protein solution and (D) MN material solution.

rication [20,21]. Thus, evaluation of the insertion capability of the H7N9 loaded dissolving MNs was essential. No wound was present on the porcine ear skin after MN removal (Fig. 2A). Fig. 2B–D shows the skin condition under optical and fluorescence microscopy. When rhodamine B loaded MNs are inserted into porcine skin, the rhodamine B diffuses rapidly into the skin. Under a CLSM, the skin into which the MNs were inserted demonstrated gradually declining fluorescence intensity with increasing depth. Fig. 4E is a 3D confocal image, with the z axis showing that the MN depth was 280 μm. These images indicate that the MNs pierced and overcame the elastic skin barrier.

3.2. Structural integrity of the influenza H7N9 vaccine structure during MN fabrication

To examine the structural integrity of the encapsulated influenza H7N9 virus during fabrication, we compared the H7N9 vaccine structure before and after encapsulation with coating materials. Fig. 3A shows the structure of the H7N9 vaccine. Fig. 3B shows the H7N9 vaccine structure in the matrix solution under an EM. The H7N9 vaccine formed a cluster after encapsulation, causing the aggregation of protein particles.

3.3. Size distribution and biological distribution of the influenza H7N9 virus during MN fabrication

DLS was used to detect aggregates with sizes ranging from 1 nm to 1 μm [22]. Fig. 3C and D shows that the native influenza H7N9 vaccine particles have a mean diameter of 167.8 nm. After encapsulation, the H7N9 vaccine particles had a mean diameter of 376.6 nm, with greater size and particle size distribution than before encapsulation, suggesting that the H7N9 vaccine protein agglomerates in MNs.

To identify the H7N9 distribution after administration by IM injection and MNs, BALB/c mice underwent IVIS testing at 6 h and 3, 5, and 8 days. Fig. 4A shows the fluorescence distribution of Cy-7. Cy-7 showed stronger and longer duration of fluorescent signals on the skin site at 6 h and 3, 5, and 8 days after MN administration relative to after IM administration, indicating that the

antigen remained in the target region for a longer duration after MN compared with IM administration.

3.4. Humoral and cellular immunity

The immune responses induced by dissolving MNs and IM injection were compared. Serum was collected on day 14 after booster immunization. The antibody responses and HI titers against the influenza H7N9 virus were examined. No significant difference between the MN and IM groups was observed in HI (p = 0.06) or the IgG level (p = 0.067; Fig. 5A). These results indicate that the MN and IM immunizations induced similar levels of functional antibody production.

The IgG1 level did not differ significantly between MN and IM administration, but the IgG2a level was higher in the IM than in the MN group (Fig. 5C). The IL-4 level did not differ significantly between the IM and MN groups, but the IFN-γ level was higher in the MN than in the IM group (Fig. 5D, E). The results of higher IFN-γ and trend towards lower IL-4 would actually suggest a Th1-biased immune response in mice.

3.5. Changes in survival rate and body weight after challenge

Influenza H7N9 vaccine delivery by MNs induced strong immune responses with significant HI titers after booster vaccination. In addition, we evaluated whether the BALB/C mice were protected from the influenza H7N9 virus. At 2 weeks after vaccination, the mice were challenged with 0.7×10^6 PFU/ml influenza virus A/Anhui/1/2013 (H7N9). The control group showed > 25% body weight loss (Fig. 6A), whereas body weights were reduced by only 5% in the MN group and 10% in the IM group. The control mice were killed 4–8 days after the challenge. All immunized mice survived the virus challenge (Fig. 6B). Though there were no significance of viral titers in lung lavage fluid between MN and IM administration, the MN group have lower viral titers than Control group (Fig. 6C). These results suggest that vaccination via MN and IM administration protected the mice against the influenza H7N9 virus, but that MN administration was associated with lower virus levels in lung lavage fluid than was Control administration.

(A)   (B)
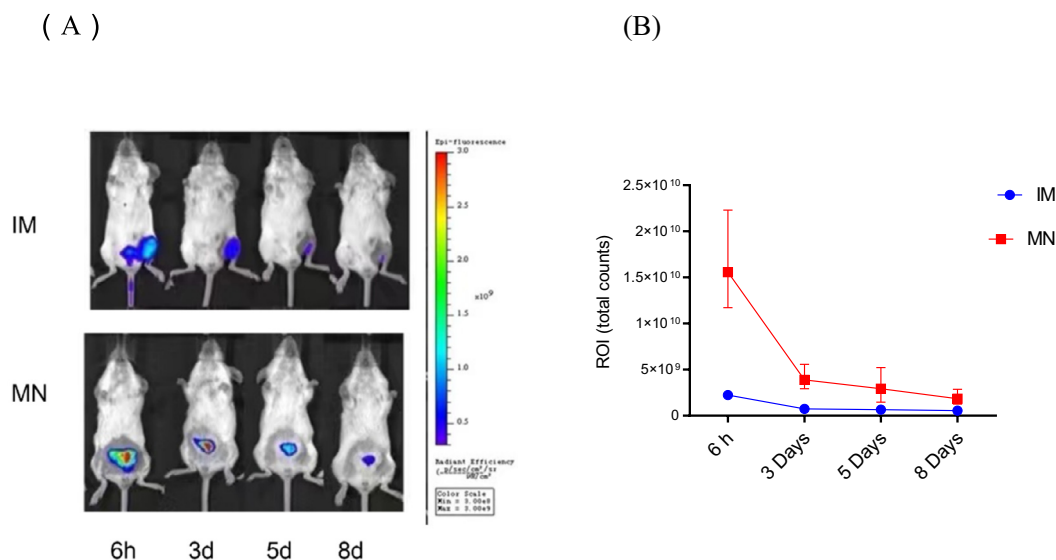
Fig. 4. Fluorescence intensity after microneedle (MN) or intramuscular (IM) administration of Cy-7 labeled H7N9 antigen protein at different timepoints. (A) In vivo fluorescence images of BALB/c mice at 6 h and 3, 5, and 8 days after treatment with Cy-7 labeled H7N9 antigen protein loaded MNs (n = 3/group). (B) Fluorescence intensity was evaluated at 6 h and 3, 5, and 8 days after administration (ROI, region of interest).
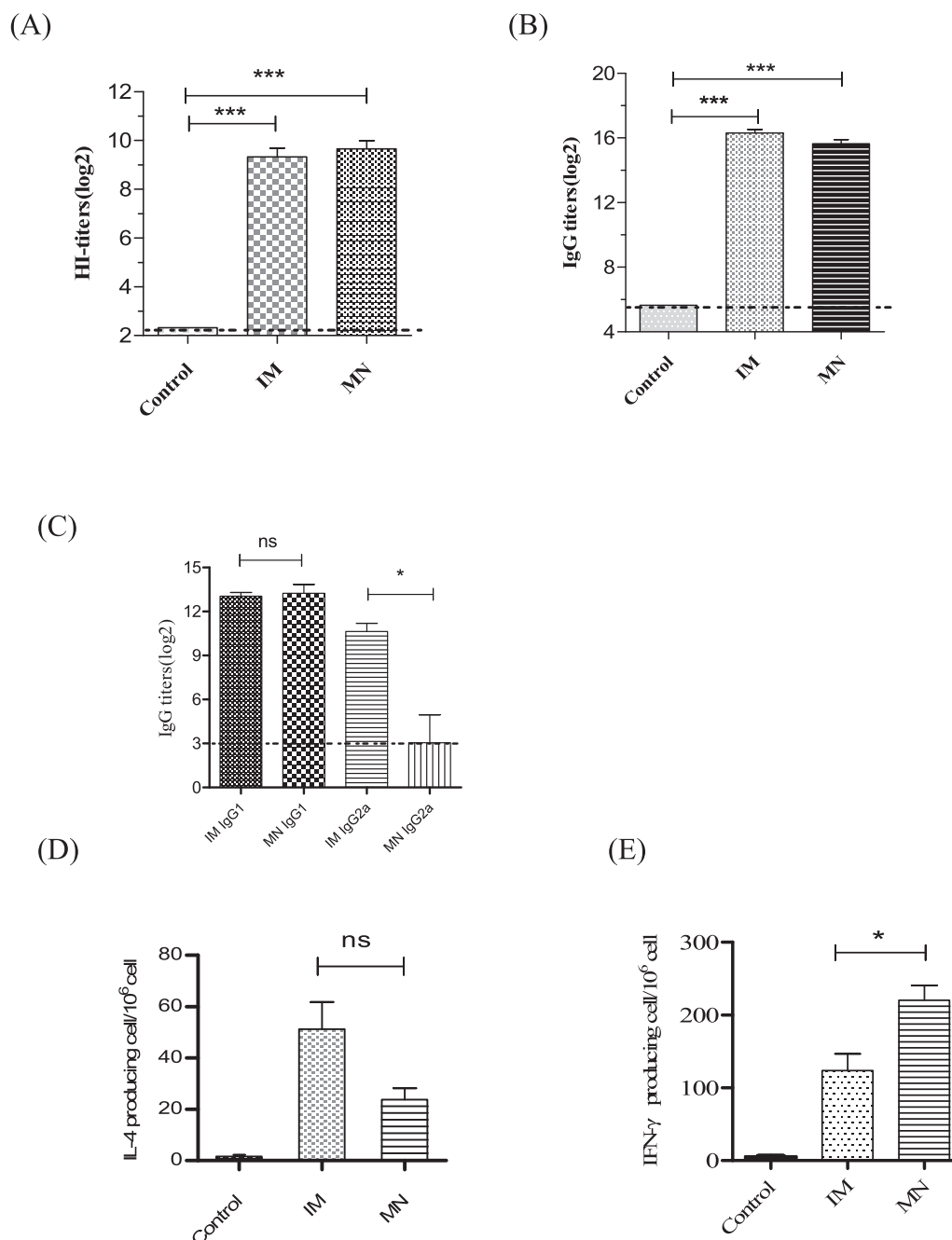
Fig. 5. **Immune response after H7N9 vaccine administration by microneedles (MNs) and intramuscular (IM) injection.** (A) Hemagglutination inhibition (HI) titers detected 14 days after booster immunization via IM and MN administration. (B) Serum IgG level, detected by enzyme-linked immunosorbent assay (ELISA). (C) Serum IgG1 and 2a titers, detected by ELISA. (D) Level of IL-4 secreted by cells after immunization. (E) Level of IFN-γ secreted by cells after immunization. The 6–8-week old BALB/c mice (n = 6/group) were immunized with influenza virus (A/Anhui/1/2013) vaccine via IM or MN administration, and phosphate-buffered saline (PBS) was administered through IM injection in the control group. Control, PBS group. Data are means ± standard errors of the mean. (*p < 0.01, ***p < 0.001, ns: no significance).

3.6. Inflammatory histopathological changes after virus challenge

The histopathological lesions observed 4 days after virus inoculation varied among the groups (Fig. 7). MN treated mice demonstrated minimal lesions. The control group showed microscopic lung lesions reflecting conditions such as severe bronchiolitis, alveolitis, and lung damage, including peribronchiolar and perivascular lymphocytic infiltration. Based on gross and microscopic lesion examination, IM and MN vaccination protected the mice's lungs against influenza H7N9 virus infection.

4. Discussion

The outbreak of severe acute respiratory syndrome coronavirus 2 infection in 2019 has generated widespread interest in emerging viruses, such as avian H7N9 [23]. The use of MN to administer inactivated influenza vaccines against the H1N1, H3N2, and B strains was evaluated in a phase I clinical trial [24,25]. Other studies have demonstrated the prolonged (for up to 3 months) stability of dissolving MNs loaded with influenza vaccines [26]. To achieve the immune response, vaccine doses can be increased by increasing
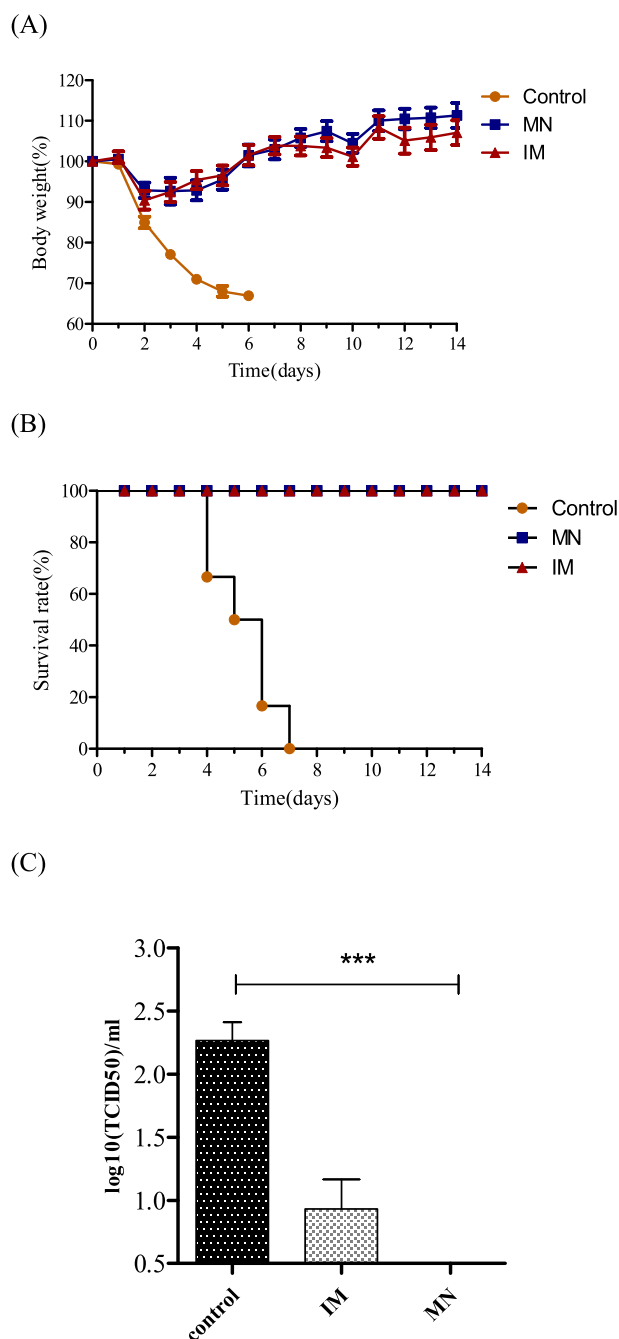
Fig. 6. Survival rate, weight loss, and TCID50 of mice after virus challenge. (A) Body weight and (B) survival rate after virus challenge. (n = 7) (C) Virus load in lung lavage fluid, detected by TCID50 assay (n = 3).

the MN array size and number of needles per array [27]. In the present study, we investigated transcutaneous immunization against influenza H7N9 MNs harbouring 196 needles per array. These dissolving MNs are composed of a matrix solution containing chondroitin sulfate, hydroxypropyl methylcellulose, and trehalose.

Dissolving MNs deliver vaccines to skin antigen-presenting cells to achieve transcutaneous immunization [28]. Antigen presentation by dendritic cells, similar to Langerhans cells, results in the delivery of antigens to the epidermis, which is the MN target site [29]. In our study the IVIS testing showed that antigen delivery and transmission through MNs led to slow vaccine release, which increases the duration of the effect. Based on the structural integrity and size distribution of MNs, we assume that agglomerated proteins are better delivered by antigen-presenting cells; however, whether the intrinsic activity of agglomerated proteins is retained remains unclear. A previous study showed that drug coating fabrication can reduce antigen activity [30]. A superior method for *in vitro* antigen activity detection is needed. Recent studies suggest that the quantification of antigens released in the skin is difficult because of variation due to the dissolvability of the MN patch [31]. Thus, it is also required a standardized method for such quantification. What's more, further studies should be conducted with the use of other methods to develop optimized MN formulations and evaluate the long term stability of influenza H7N9 loaded MNs.

In general, at present influenza H7N9 vaccine with adjuvant may regarded as the most option for controlling the pandemic [32]. Herein, we in the first time report H7N9-loaded microneedles which enrich the H7N9 vaccine options. Transcutaneous immunization may stimulate skin effector T cells, which is important for transcutaneous antigen administration and is not achieved by IM administration [33]. Our results indicate that the influenza H7N9 vaccine can be delivered efficiently into mouse skin via MNs, and that this approach induces humoral responses similar to those achieved with IM administration. In future studies, microneutralization or plaque reduction assays should be used to compare the levels of antibodies induced by IM and MN administration. The antibody results showed the level of IgG2a is significantly lower for the MN vaccine than the IM, and there was no real difference in the IgG1. It would be expected that the total IgG level was also lower, yet it was not. We assumed that the total IgG could be influenced by other subsets resulting in the results of our study. Furthermore, it seems contradictory that the MN inoculation induced lower IgG2a antibodies, yet more T cells that secrete IFN-γ. In mice, T helper (Th)1-dependent IFN-γ induces the production of IgG2a, and the Th2 cytokine IL-4 induces the production of IgG1 [34], but the relationship between Th1 and IgG2a is not absolute. The lower IgG2a should not be taken to mean that MN injection induces a greater Th2 than Th1 immune response, however. If anything, the Th1 versus Th2 label should rely more on the actual T cell cytokine production than on antibody isotype, and the higher IFN-γ and trend towards lower IL-4 would actually suggest a Th1-biased immune response in vivo. For the next step,
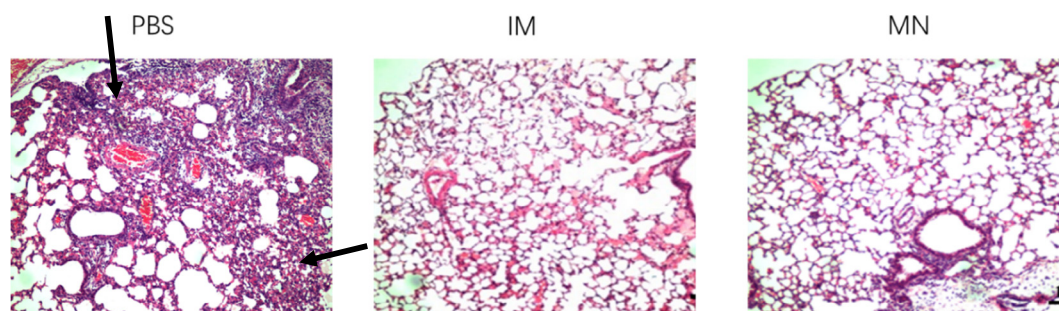
Fig. 7. Pathological characteristics after virus challenge. Hematoxylin and eosin stained histopathological sections showing inflammatory changes in the control, intramuscular (IM) injection, and microneedle (MN) administration groups. The arrows show the inflammatory cell infiltration in the pathological lung of the PBS group (10 × magnification under an optical microscope (Leica, Germany)).

we will perform the flow cytometry panel in our subsequent study to confirm the ELISA results.

Taken together, our findings suggest that MNs represent a potential strategy for the delivery of influenza H7N9 vaccines, which overcomes several of the limitations of previous strategies. However, further preclinical and clinical studies are required to optimize MN vaccine administration.

CRediT authorship contribution statement

Siqi Liu: Methodology, Writing – original draft, Writing – original draft. **Guozhong Yang:** Conceptualization, Methodology, Resources. **Minghui Li:** Conceptualization, Methodology, Formal analysis, Writing – original draft. **Fang Sun:** Conceptualization, Methodology. **Yufeng Li:** . **Xiliang Wang:** Conceptualization, Project administration, Funding acquisition. **Yunhua Gao:** Conceptualization, Resources, Project administration. **Penghui Yang:** Conceptualization, Formal analysis, Writing – original draft, Project administration, Funding acquisition.

Declaration of Competing Interest

The authors declare that they have no known competing financial interests or personal relationships that could have appeared to influence the work reported in this paper.

Acknowledgement

Appendix A. Supplementary data

Supplementary data to this article can be found online at https://doi.org/10.1016/j.vaccine.2022.09.008.

References

[1] Wu J, Lu J, Faria NR, Zeng X, Song Y, Zou L, et al. Effect of live poultry market interventions on influenza A(H7N9) virus, Guangdong, China. Emerg Infect Dis 2016;22(12):2104–12.

[2] Fan M, Huang B, Wang Ao, Deng L, Wu D, Lu X, et al. Human influenza A(H7N9) virus infection associated with poultry farm, Northeastern China. Emerg Infect Dis 2014;20(11):1902–5.

[3] Wu X, Xiao L, Li L. Research progress on human infection with avian influenza H7N9. Front Med 2020;14(1):8–20.

[4] Kile JC, Ren R, Liu L, Greene CM, Roguski K, Iuliano AD, et al. Update: Increase in Human Infections with Novel Asian Lineage Avian Influenza A(H7N9) Viruses During the Fifth Epidemic - China, October 1, 2016-August 7, 2017. MMWR Morb Mortal Wkly Rep 2017;66(35):928–32.

[5] Liu WJ, Xiao H, Dai L, Liu Di, Chen J, Qi X, et al. Avian influenza A (H7N9) virus: from low pathogenic to highly pathogenic. Front Med 2021;15(4):507–27.

[6] Koutsakos M, Kedzierska K, Subbarao K. Immune Responses to Avian Influenza Viruses. J Immunol 2019;202(2):382–91.

[7] Guo Z, Xiao D, Li D, Wang Y, Yan T, Dai B, et al. The temporal distribution of new H7N9 avian influenza infections based on laboratory-confirmed cases in Mainland China, 2013–2017. Sci Rep 2018;8(1):4051.

[8] de Vries R, Herfst S, Richard M. Avian Influenza A Virus Pandemic Preparedness and Vaccine Development. Vaccines (Basel) 2018;6(3):46.

[9] Li C, Chen H. H7N9 Influenza Virus in China. Cold Spring Harb Perspect Med 2021;11(8):a038349.

[10] Pushko P, Tretyakova I. Influenza Virus Like Particles (VLPs): Opportunities for H7N9 Vaccine Development. Viruses 2020;12(5):518.

[11] Kim YC, Park JH, Prausnitz MR. Microneedles for drug and vaccine delivery. Adv Drug Deliv Rev 2012;64(14):1547–68.

[12] Romani N, Flacher V, Tripp CH, Sparber F, Ebner S, Stoitzner P. Targeting skin dendritic cells to improve intradermal vaccination. Curr Top Microbiol Immunol 2012;351:113–38.

[13] Lee KJ, Jeong SS, Roh DH, Kim DY, Choi HK, Lee EH. A practical guide to the development of microneedle systems - In clinical trials or on the market. Int J Pharm 2020; 573:118778.

[14] Aldawood FK, Andar A, Desai S. A comprehensive review of microneedles: types, materials, processes, characterizations and applications. Polymers (Basel) 2021;13(16):2815.

[15] Liu S, Zhang S, Duan Y, Niu Y, Gu H, Zhao Z, et al. Transcutaneous immunization of recombinant Staphylococcal enterotoxin B protein using a dissolving microneedle provides potent protection against lethal enterotoxin challenge. Vaccine 2019;37(29):3810–9.

[16] Zhu Z, Ye X, Ku Z, Liu Q, Shen C, Luo H, et al. Transcutaneous immunization via rapidly dissolvable microneedles protects against hand-foot-and-mouth disease caused by enterovirus 71. J Control Release 2016;243:291–302.

[17] Kolluru C, Gomaa Y, Prausnitz MR. Development of a thermostable microneedle patch for polio vaccination. Drug Deliv Transl Res 2019;9(1):192–203.

[18] Duong HTT, Yin Y, Thambi T, Kim BS, Jeong JH, Lee DS. Highly potent intradermal vaccination by an array of dissolving microneedle polypeptide cocktails for cancer immunotherapy. J Mater Chem B 2020;8(6):1171–81.

[19] Liu K, Yao Z, Zhang L, Li J, Xing L, Wang X. MDCK cell-cultured influenza virus vaccine protects mice from lethal challenge with different influenza viruses. Appl Microbiol Biotechnol 2012;94(5):1173–9.

[20] He M, Yang G, Zhang S, Zhao X, Gao Y. Dissolving Microneedles Loaded With Etonogestrel Microcrystal Particles for Intradermal Sustained Delivery. J Pharm Sci 2018;107(4):1037–45.

[21] Mistilis MJ, Joyce JC, Esser ES, Skountzou I, Compans RW, Bommarius AS, et al. Long-term stability of influenza vaccine in a dissolving microneedle patch. Drug Deliv Transl Res 2017;7(2):195–205.

[22] Jacobse J, Voorde W, Tandon A, Romeijn SG, Grievink HW, Maaden K, et al. Comprehensive evaluation of microneedle-based intradermal adalimumab delivery vs. subcutaneous administration: results of a randomized controlled clinical trial. Br J Clin Pharmacol 2021;87(8):3162–76.

[23] Chang YS. Coronavirus disease 2019 (COVID-19) and Long COVID. Asia Pac Allergy 2022;12(2):e22.

[24] Rouphael NG, Paine M, Mosley R, Henry S, McAllister DV, Kalluri H, et al. The safety, immunogenicity, and acceptability of inactivated influenza vaccine delivered by microneedle patch (TIV-MNP 2015): a randomised, partly blinded, placebo-controlled, phase 1 trial. Lancet 2017;390(10095):649–58.

[25] Frew PM, Paine MB, Rouphael N, Schamel J, Chung Y, Mulligan MJ, et al. Acceptability of an inactivated influenza vaccine delivered by microneedle patch: Results from a phase I clinical trial of safety, reactogenicity, and immunogenicity. Vaccine 2020;38(45):7175–81.

[26] Chu LY, Ye L, Dong K, Compans RW, Yang CL, Prausnitz MR. Enhanced Stability of Inactivated Influenza Vaccine Encapsulated in Dissolving Microneedle Patches. Pharm Res-Dordr 2016;33(4):868–78.

[27] Zhu Q, Zarnitsyn VG, Ye L, Wen Z, Gao Y, Pan L, et al. Immunization by vaccine-coated microneedle arrays protects against lethal influenza virus challenge. P Natl Acad Sci USA 2009;106(19):7968–73.

[28] Sullivan SP, Koutsonanos DG, del Pilar Martin M, Lee JW, Zarnitsyn V, Choi S-O, et al. Dissolving polymer microneedle patches for influenza vaccination. Nat Med 2010;16(8):915–20.

[29] Clayton K, Vallejo AF, Davies J, Sirvent S, Polak ME. Langerhans Cells-Programmed by the Epidermis. Front Immunol 2017;8.

[30] Kim YC, Quan FS, Compans RW, Kang SM, Prausnitz MR. Formulation and coating of microneedles with inactivated influenza virus to improve vaccine stability and immunogenicity. J Control Release 2010;142(2):187–95.

[31] Leone M, Monkare J, Bouwstra J, Kersten G. Dissolving microneedle patches for dermal vaccination. Pharm Res-Dordr 2017;34(11):2223–40.

[32] Zheng D, Gao F, Zhao C, Ding Y, Cao Y, Yang T, et al. Comparative effectiveness of H7N9 vaccines in healthy individuals. Hum Vaccin Immunother 2019;15 (1):80–90.

[33] Karande P, Mitragotri S. Transcutaneous immunization: an overview of advantages, disease targets, vaccines, and delivery technologies. Annu Rev Chem Biomol 2010;1(1):175–201.

[34] Firacative C, Gressler AE, Schubert K, Schulze B, Müller U, Brombacher F, et al. Identification of T helper (Th)1-and Th2-associated antigens of Cryptococcus neoformans in a murine model of pulmonary infection. Sci Rep-Uk 2018;8(1).